

Journal Pre-proof

Molecular modeling to elucidate the dynamic interaction process and aggregation mechanism between natural organic matters and nanoplastics

Chi Zhang, Zhiyu Zhou, Mengning Xi, Haozhe Ma, Junhao Qin, Hanzhong Jia



PII: S2772-9850(24)00060-7

DOI: <https://doi.org/10.1016/j.eehl.2024.08.004>

Reference: EEHL 122

To appear in: *Eco-Environment & Health*

Received Date: 24 May 2024

Revised Date: 25 August 2024

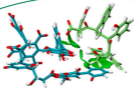
Accepted Date: 30 August 2024

Please cite this article as: C. Zhang, Z. Zhou, M. Xi, H. Ma, J. Qin, H. Jia, Molecular modeling to elucidate the dynamic interaction process and aggregation mechanism between natural organic matters and nanoplastics, *Eco-Environment & Health*, <https://doi.org/10.1016/j.eehl.2024.08.004>.

This is a PDF file of an article that has undergone enhancements after acceptance, such as the addition of a cover page and metadata, and formatting for readability, but it is not yet the definitive version of record. This version will undergo additional copyediting, typesetting and review before it is published in its final form, but we are providing this version to give early visibility of the article. Please note that, during the production process, errors may be discovered which could affect the content, and all legal disclaimers that apply to the journal pertain.

© 2024 The Author(s). Published by Elsevier B.V. on behalf of Nanjing Institute of Environmental Sciences, Ministry of Ecology and Environment (MEE) & Nanjing University.

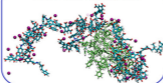
Weak interaction



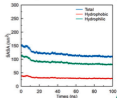
Surface reactivity



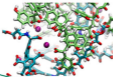
NOMs-NPs aggregation



Dynamic process



Ca bridging



1 **Molecular modeling to elucidate the dynamic interaction**
2 **process and aggregation mechanism between natural organic**
3 **matters and nanoplastics**

4 Chi Zhang ^{a,b,1}, Zhiyu Zhou ^{a,1}, Mengning Xi ^a, Haozhe Ma ^a, Junhao Qin ^{c,*},
5 Hanzhong Jia ^{a,b,*}

6 ^a College of Natural Resources and Environment, Northwest A & F University, Xianyang 712100,
7 China

8 ^b Key Laboratory of Low-Carbon Green Agriculture in Northwestern China, Ministry of
9 Agriculture and Rural Affairs, Xianyang 712100, China

10 ^c Guangdong Laboratory for Lingnan Modern Agriculture, Guangdong Provincial Key Laboratory
11 of Agricultural & Rural Pollution Abatement and Environmental Safety, College of Natural
12 Resources and Environment, South China Agricultural University, Guangzhou 510642, China

13
14
15 ¹ Contributed equally to this work

16 *Corresponding authors

17 E-mails: J_Qin@scau.edu.cn (J. Qin); jiahz@nwafu.edu.cn (H. Jia)

18

19

20

21

22

23

24

25

26

27

28 **Abstract**

29 The interactions of nanoplastics (NPs) with natural organic materials (NOMs)
30 dominate the environmental fate of both substances and the organic carbon cycle. Their
31 binding and aggregation mechanisms at the molecular level remain elusive due to the
32 high structural complexity of NOMs and aged NPs. Molecular modeling was used to
33 understand the detailed dynamic interaction mechanism between NOMs and NPs.
34 Advanced humic acid models were used, and three types of NPs, i.e., polyethylene (PE),
35 polyvinyl chloride (PVC), and polystyrene (PS), were investigated. Molecular
36 dynamics (MD) simulations revealed the geometrical change of the spontaneous
37 formation of NOMs-NPs supramolecular assemblies. The results showed that pristine
38 NPs initially tend to aggregate homogeneously due to their hydrophobic nature, and
39 then NOM fragments are bound to the formed NP aggregates mainly by vdW interaction.
40 Homo- and hetero-aggregation between NOMs and aged NPs occur simultaneously
41 through various mechanisms, including intermolecular forces and Ca^{2+} bridging effect,
42 eventually resulting in a mixture of supramolecular structures. Density functional
43 theory calculations were employed to characterize the surface properties and reactivity
44 of the NP monomers. The molecular polarity indices for unaged PE, PS, and PVC were
45 3.1, 8.5, and 22.2 kcal/mol, respectively, which increased to 43.2, 51.6, and 42.2
46 kcal/mol for aged NPs, respectively, indicating the increase in polarity after aging. The
47 vdW and electrostatic potentials of NP monomers were visualized. These results
48 clarified the fundamental aggregation processes, and mechanisms between NPs and
49 NOMs, providing a complete molecular picture of the interactions of nanoparticles in
50 the natural aquatic environment.

51 **Keywords:** Natural organic matters; Aged nanoplastics; Interaction processes;
52 Aggregation mechanism; Molecular modeling

53

54 1. Introduction

55 Natural organic matters (NOMs) play a critical role in a variety of
56 (bio)geochemical processes in natural water environments by directly affecting
57 microbial activity, co-aggregation, contaminant retention, water quality, and element
58 cycling. The environmental behaviors of NOMs are also closely related to the global
59 carbon cycle and climate change by preserving and converting organic carbon [1, 2].
60 Despite their importance, a thorough and precise understanding of NOMs' composition
61 and structure is still lacking. Structurally, NOM is extremely complex and
62 heterogeneous as a supramolecular mixture of chemically distinct organic compounds
63 that are abundant in chemically diverse functional groups and active sites. The major
64 functional groups in NOM have long been clearly identified, such as carboxylic,
65 phenolic, alcoholic, carbonyl, amino, etc. The compositional complexity and structural
66 diversity of NOMs present a severe challenge to experimental characterization and
67 building of realistic models, but nowadays computational chemistry methods have
68 made this problem tractable [3-5].

69 In nature, NOMs interact closely with organic pollutants through mechanisms such
70 as adsorption, co-precipitation, and homogeneous/heterogeneous aggregation through
71 different mechanisms such as π - π interaction, hydrophobic interaction, H-bonding,
72 electrostatic attraction, steric hindrance effect, and so forth [6], thus governing the
73 environmental fate of pollutants and profoundly impacting the distribution and
74 preservation of organic carbon. Nanoplastics (NPs), as a class of emerging
75 contaminants, have a particle size between 1 nm and 100 nm [7] and are generated from
76 plastic production by natural or anthropogenic factors, such as photooxidation and
77 microbial degradation [8, 9]. Due to their chemical stability, persistence, and
78 bioaccumulation, the environmental behaviors of NPs, in particular their interactions
79 with different environmental pollutants during their transport through the marine or
80 sedimentary environment into ecosystems, have received considerable research
81 attention in recent years [10-13]. Compared to microplastics (MPs, <5mm), the

82 molecular-level properties and environmental implications of NPs in natural systems
83 have been relatively less studied because of methodological challenges. For instance, it
84 is still technically challenging to extract NPs from natural environments, and their
85 surface properties are not clearly identified [14-17]. There is also research suggesting
86 that NPs are more abundant and hazardous in the environment than MPs [18]. The
87 transport and fate of NPs are greatly determined by interactions with environmental
88 media, such as aggregation with NOMs and deposition onto minerals' surfaces [19-22].
89 Therefore, it is imperative to understand the environmental processes and behaviors of
90 NPs with environmental media, thus providing significant implications for their
91 ecological risk assessment.

92 The interactions between NOMs and NPs are of fundamental importance and
93 largely control the environmental fate of both materials, as well as the stabilization and
94 cycling of organic carbon in nature [23]. NOMs can have an impact on the transport
95 and distribution of NPs in the aquatic environment, because the presence of NOMs can
96 alter the surface properties of NPs, affecting their aggregation and mobility [24]. NOM
97 can also be adsorbed onto the surface of NPs, changing their chemical reactivity and
98 affecting the adsorption of other contaminants, such as metals and organic pollutants,
99 onto the NP surface [25]. Furthermore, the evaluation of the effect of NOMs on the
100 behaviors of NPs was the first critical step in assessing the potential environmental
101 hazards of NPs in ecosystems. However, a detailed molecular-level picture of the
102 dynamic interaction processes and the underlying mechanism between NOMs and NPs
103 is still elusive. It is difficult to directly observe and decipher the complicated NOM–NP
104 aggregating behaviors only relying on traditional experimental techniques. There is an
105 urgent need for a better understanding of such processes that can provide more
106 quantitative information, such as the determination of fundamental mechanisms
107 (homo–aggregation or hetero–aggregation), identification of active sites, observation
108 of dynamic aggregation processes, and characterization of binding and aggregating
109 structures.

110 With the rapid development of theoretical and computational chemistry and
111 computer hardware, computational simulations have been proven an essential and
112 powerful approach in quantitatively revealing aqueous environmental processes and
113 reactions at the molecular scale beyond the conventional resolution of analytical
114 methods, based on the identification and analysis of a range of physicochemical
115 properties, such as geometrical characteristics, thermodynamics, electronic structures,
116 and dynamics of substances [5, 26-33]. For example, Xue et al. [34] reviewed the
117 application of computational modeling methods at various scales in understanding the
118 interface behavior of pollutants, especially in aquatic environments. Li et al. [31]
119 reviewed recent progress in using environmental theoretical calculations to elucidate
120 the transformation mechanisms of contaminants. In addition, this group has extensively
121 revisited the application of density functional theory (DFT) calculations to the
122 prediction of active sites and reaction selectivity, as well as oxidant activation
123 mechanisms in the field of advanced oxidation processes (AOPs) [30]. However,
124 research providing deep insights into the interactions between NOMs and NPs has
125 rarely been conducted using theoretical calculation methods. In a recent study, the
126 dynamic properties and microscopic aggregation structures related to the NPs-NOMs
127 assemblage were studied by molecular dynamics (MD) simulations, which acquired
128 deep insights into the interparticle interactions between both substances [35]. However,
129 this study only incorporated virgin plastics, and the aged forms of NPs were not
130 considered. According to previous research [23,36-38], oxygen-containing functional
131 groups, including carboxyl, phenolic, and carbonyl groups, are generated after aging,
132 which leads to the modification of the surface morphology of MPs, such as specific
133 surface area and roughness. Therefore, it can be expected that different surface
134 properties of aged NPs would lead to more significant and interesting phenomena and
135 aggregation mechanisms with NOMs in comparison to pristine NPs, given that NOMs
136 have a high degree of structural complexity and heterogeneity, the chemical
137 composition of which is very diverse, and aged NPs also have a wide variety of O–

138 containing functional groups.

139 In the present study, by performing MD simulations and DFT calculations, we
140 explored the dynamic interactions and elucidated the detailed molecular-level
141 mechanism between NOMs and three types of NPs, polyethylene (PE), polyvinyl
142 chloride (PVC), and polystyrene (PS) in both pristine and aged form. The dynamic
143 binding and aggregation processes between two substances are qualitatively revealed
144 by the movement trajectories and statistical data. Analysis of the interaction energies
145 between NOM and NP fragments and characterization of the direct intermolecular
146 binding and local coordination geometries of Ca^{2+} bridging provides a profound insight
147 into the aggregation mechanism. DFT calculations allow a quantitative analysis of the
148 reactivity and active sites of NPs, and weak interactions between NOM and PS
149 fragments are presented visually. These results establish a fundamental basis for the
150 understanding of the fate of NPs in the aquatic environment and the stabilization of
151 organic C.

152 **2. Methodology**

153 **2.1. Computational models**

154 **2.1.1. Leonardite humic acid**

155 Vienna Soil Organic Matters Modeler 2 (VSOMM2) is an online tool to generate
156 theoretical models of humic substances [39, 40] based on the data derived from
157 standardized samples of the International Humic Substances Society (IHSS). The
158 NOMs condensed phase models constructed by VSOMM2 fundamentally rely on the
159 concept of building blocks (BBs), which represent the simple units in organic
160 components, and the implementation of a genetic algorithm randomly results in the
161 chemical and structural diversity of the final models. On this website, the primary
162 elemental composition and organic carbon fractions are required as input, and the
163 modeler calculates and generates a diverse combination of heterogeneously distributed

164 NOM fragments automatically that match the input.

165 In this study, VSOMM2 was used to build theoretical models of the supramolecular
166 structure of Leonardite humic acid (LHA) according to the elemental and organic
167 composition of the IHSS. LHA has been extensively used in the molecular modeling of
168 NOMs in previous studies [5, 27]. The created LHA model was composed of 100
169 building blocks with 10 building blocks per molecule. The detailed element and organic
170 composition of the generated LHA are listed in Table S1. The molecular geometries of
171 the 10 deprotonated NOM fragments are illustrated in Fig. S1. These molecules
172 collectively constitute the NOMs' supramolecular association.

173 **2.1.2. Nanoplastics**

174 Both pristine and aged NPs (Fig. S2) were investigated in our simulations with the
175 purpose of clarifying the effect of oxygen-containing functional groups on aggregation
176 behaviors. Each monomer of the PE and PVC chain had a degree of polymerization of
177 10, and each PS monomeric chain contained 5 polymerized units. There were 16 such
178 NP monomers in each simulation system. For pristine NPs, the models we used were
179 similar to those in previous studies. For aged NPs, due to their structural complexity,
180 the models have not yet been developed, so we had to use the simplified models.
181 Simplified models of aged NPs were constructed by incorporating O-containing
182 functional groups according to previous studies [35, 41]. In brief, each monomer
183 contained four carbonyls, two hydroxyls, and one carboxyl. The carboxylic groups of
184 NOM and NP fragments were deprotonated (in a circumneutral environment) due to the
185 relatively low pK_a of these groups. Each monomeric chain of aged NPs possessed a net
186 charge of -1, and the 10 NOM fragments had different negative charges depending on
187 the number of carboxylate groups.

188 **2.1.3. Simulation systems**

189 NOMs–NPs coexisting binary systems (Fig. 1) were constructed. NOMs and NPs
190 molecules were initially placed at random positions within the simulation cell. This

191 setup was designed to enable the direct observation of the spontaneous aggregation
192 processes of both materials. Alternatively, one can first build a homo-aggregate of NP
193 nanoparticles, then possibly age its surface, and then insert these NOM molecules into
194 the solution. This setup should be more reasonable but also more complicated and
195 therefore not adopted in this work. Moreover, to clearly reveal the effect of their
196 interactions on the behaviors of both NOMs and NPs, unary systems that contained
197 only NOMs or NPs were also simulated. There were 13 individual simulation systems
198 in all: 6 binary systems and 7 unitary systems. For each system, NOM/NP fragments
199 were first randomly distributed in the simulation box (approximately $76.5\text{\AA} \times 76.5\text{\AA} \times$
200 76.5\AA), and then salt ions and solvent water molecules were randomly placed in the
201 region to simulate the solution environment. It is well known that Ca^{2+} and Na^+ are the
202 most common salt ions. Therefore, Ca^{2+} ions were added to counterbalance the net
203 negative charges from NOMs and aged NPs, and additionally ~ 0.1 mol/L NaCl was
204 added in each system. The detailed compositions of all the systems are summarized in
205 Table S2. All of the simulation cells were periodically repeated.

206

207 **Fig. 1.** Computational models of original systems used for MD simulations. NOMs and
208 NPs fragments are shown as sticks; salt ions are represented by balls. Color code: N =
209 blue; H = white; O = red; S = yellow; Na = green; Ca = purple; Cl = orange. The C in
210 NOMs and NPs are colored by cyan and brown, respectively. The water molecules are
211 not shown for clarity.

212

213 2.2 MD setup

214 All MD simulations were carried out by GROMACS 2018.4 [42]. Amber 03 force
215 field [43] was used to describe interatomic interactions. A cutoff value of 12\AA was used
216 for short-range electrostatic and van der Waals (vdW) interactions. The PME
217 summation method [44] was employed for the summation of long-range electrostatic
218 interactions. The SPC/E water model was used [45]. The rigidity of water was
219 constrained by the LINCS algorithm [46]. The atomic charges were derived by DFT

220 calculations (see the details in *Section 2.3*).

221 The propagation of Newtonian equations of motion was realized via the leap-frog
222 algorithm. Berendsen barostat [47] and velocity-rescale thermostat [48] were employed
223 to maintain the pressure and temperature, respectively. For each simulation, we first
224 performed a pre-equilibration for 0.5 ns in the NVT ensemble at 298 K and then 1–2 ns
225 equilibration in the NPT ensemble at 1 atm and 298 K. Subsequently, a production run
226 for 100 ns with a timestep of 2 fs in NVT ensemble was carried out. Data of the last 20
227 ns were used for statistics.

228 **2.3 DFT calculations for surface reactivity**

229 DFT calculations were used to give a more comprehensive understanding of the
230 interaction mechanism at atomic and electronic scales. All of the quantum chemistry
231 calculations were conducted by the Gaussian 16 program. The geometry optimizations
232 of the 6 monomeric chains of NPs (i.e., pristine and aged PE, PVC, and PS) and 10
233 individual NOM fragments were performed at the quantum chemistry level of def2-
234 TZVP basis set [49] and B3LYP functional [50, 51], complemented by DFT–D3
235 dispersion correction [52]. The partial atomic charges of all the NOMs and NP
236 monomers were derived by the Multifwn 3.8 program [53]. The acquired RESP2 (0.5)
237 atomic charges [54] were used in MD simulations.

238 Several key descriptors were analyzed on the basis of the structures and
239 wavefunctions by Multifwn 3.8 [53], including electrostatic potential (ESP), vdW
240 potential, and molecular polarity index (MPI) of NP monomers. ESP is quite common
241 and useful for intuitively disclosing possible electrostatic interaction of the investigated
242 chemical entity with the external environment, and ESP is usually mapped on an
243 electron density isosurface of 0.001 a.u. [55]. Due to the low polarity of pristine NPs,
244 their vdW interaction deserves more attention than electrostatic interactions. As a new
245 real space function that is similar to ESP, vdW potential can visually reflect the vdW
246 interaction between a chemical system and the external environment [56]. The
247 advantage of MPI is that it quantifies local polarity induced by the non-uniform

248 distribution of ESP, which is a better descriptor compared to dipole moment that only
249 depicts overall polarity.

250 **2.4. Weak interaction analysis and visualization**

251 An independent gradient model based on the Hirshfeld partition (IGMH) of the
252 molecular density method [57] can help to graphically display the weak interactions
253 between two fragments in a complexing system. In order to analyze the nature and
254 region of interaction between NOM and NP fragment, a configuration of a typical
255 NOM–NP dimer was optimized by DFT static calculations in a non-periodic system,
256 and IGMH analysis was performed subsequently by Multifwn 3.8 [53]. All of the
257 isosurface maps were shown and rendered by VMD software [58].

258 The geometry optimization of the dimer was conducted with the
259 CP2K/QUICKSTEP package [59], which was based on a mixed Gaussian and plane
260 waves (GPW) approach [60]. PBE exchange–correlation functional [61], DZVP basis
261 sets [62], and GTH pseudopotentials [63] were applied. The electronic density cutoff
262 was 500 Ry. L–BFGS optimizer [64] was adopted, and convergence criteria for
263 maximum force and displacement were set to be 0.0001 and 0.001 a.u., respectively.
264 Self-consistent continuum solvation (SCCS) implicit solvent model [65] and Grimme’s
265 DFT–D3 dispersion correction [52] were employed.

266 **3. Results and discussion**

267 **3.1 Dynamic aggregation processes and structures**

268 **3.1.1 Unitary systems**

269 For unitary systems, the solvent-accessible surface areas (SASAs) as a function of
270 the simulation time of individual NOMs and NPs fragments are shown in Fig. S3. One
271 can observe an overall tendency that all the SASAs are decreasing with simulation time,
272 which indicates the dynamic homo–aggregation processes with the formation of large
273 supramolecular structure (Fig. S4). Notably, the hydrophobic areas of the unaged NPs

274 decreased markedly and remained stable in later simulations, indicating the importance
275 of hydrophobic forces in the self-assembly of the NPs. As NPs molecules come into
276 contact, the water molecules between them are expelled into the bulk due to the weaker
277 interactions between water and hydrophobic surfaces, compared to interactions with
278 other solvents, which is considered an entropy-driven process [66]. Simulation
279 trajectories clearly show that separate NP monomers move toward each other
280 spontaneously and ultimately form a compact cluster. For pristine NPs, it is evident that
281 hydrophobic regions make a dominant contribution to the total SASA, while
282 hydrophilic areas make up only a very small proportion (Fig. S3A, C, E), due to the
283 hydrophobic nature of unaged NPs surfaces. Pristine PE homo-aggregate, the least
284 hydrophilic area, is nearly zero (Fig. S3A). In contrast, PVC polymer shows the largest
285 hydrophilic areas, possibly due to the slight polar property induced by Cl atoms in alkyl
286 chains (Fig. S3C), which is consistent with a previous study [44]. In contrast, the
287 hydrophilic areas of aged NPs homogeneous agglomerates (Fig. S3B, D, F) are
288 significantly larger than those of unaged NPs. This phenomenon provides evidence that
289 the oxygen-containing functional groups endow hydrocarbon molecules with partial
290 hydrophilic characteristics. All three types of pristine NPs formed stable aggregate
291 structure of a large aggregate (Fig. S4A, C, E) driven mainly by hydrophobic interaction.

292 Similar to pristine NPs, the supramolecular aggregate of aged NPs homo-
293 aggregate is gradually formed with the movement of the whole system. Aged PE
294 ultimately evolved into several small clusters (Fig. S4B) that are less compact compared
295 to the large supramolecular architecture formed by PVC and PS (Fig. S4D and F).
296 Furthermore, the homo-aggregation of aged NPs proceeds through more complicated
297 mechanisms than unaged NPs: hydrophilic (e.g., H-bonding), hydrophobic, and cation
298 bridging (via Ca^{2+}) collectively contribute to the homo-aggregation of aged NPs in a
299 water environment. In the unitary system of NOMs, the aggregation of LHA molecules
300 occurs gradually, first by forming close contacts and then by the chelation of functional
301 groups to form a co-aggregate (Fig. S4G), and its aggregation mechanism has been

302 discussed at great length in previous MD studies [3, 67-69].

303 **3.1.2 Binary systems**

304 The root-mean-square deviation (RMSD) curves of NOMs-NPs associations as a
305 function of simulation time are presented in Fig. S5. The curves show that the RMSD
306 values stabilize at approximately 4.5 nm after 40 ns, indicating that the sampling is
307 sufficient. The variations of solvent-accessible surface areas (SASAs) of NOMs-NPs
308 associations over simulation time in binary systems are shown in Fig. 2, which manifest
309 the gradual aggregation processes of NOMs and NPs mixtures for all systems. In the
310 initial configurations, the fragments of NOMs and NPs are arranged in a random
311 manner, and no significant interactions are observed between these fragments. As the
312 system moves, the distances between the NOMs and NPs decrease, driven by the
313 gradual increase in intermolecular forces and H-bonding interactions, eventually
314 leading to aggregation. Fig. 3 illustrates the microscopic geometric configurations of
315 the formed NOMs-NPs aggregates. For the NOMs-pristine PE system, all of the PE
316 monomers aggregate to form a small particle with a pillar-like geometry. In this
317 structure, the alkane chains are bundled together and aligned parallel to each other
318 through hydrophobic interactions. Subsequently, NOM fragments or small clusters are
319 adsorbed onto the external surface of the PE polymer through their hydrophobic groups.
320 Such a heterogeneous aggregation mechanism, triggered by the simultaneous
321 adsorption of NOMs and homogeneous aggregation of NPs, results in the formation of
322 a pristine NOMs-NPs PE aggregate (Fig. 3A). In this structure, the outer NOMs expose
323 their hydrophilic functional groups to the external aqueous environment, exhibiting a
324 high binding affinity to metal cations and polar organic substances. In comparison,
325 substantial heterogeneous aggregation occurs between NOMs and aged PE fragments
326 due to the increased hydrophilicity of PE. As a result, aged PE and NOMs directly form
327 hetero-aggregating structures through intermolecular interactions and cation bridging
328 (Fig. 3B). For NOMs-pristine PVC binary system, both substances polymerize
329 individually to form separate clusters, and then the two homo-aggregates are bound

330 together primarily through non-polar moieties (Fig. 3C). As shown in Fig. 3D, the case
331 for aged PVC is slightly different: the large cluster of aged PVC and supramolecular
332 aggregate of NOMs have less significant interaction in which a small portion of the
333 deprotonated carboxyl groups of aged PVC and NOMs are bridged by Ca^{2+} . For NOMs,
334 which are pristine PS binary systems, the formed agglomerate is structurally similar to
335 that of NOMs–pristine PE assemble. That is, PS monomers aggregate by hydrophobic
336 force and intense π – π stacking, and then separate NOM clusters with different
337 geometries bind to their outer surface by intermolecular interactions (Fig. 3E). NOMs
338 and aged PS directly form a large heterogeneous aggregate in which fragments of both
339 materials are joined mainly by cation bridging (Fig. 3F), similar to the case for NOMs–
340 aged PE aggregate described above. A recent study has demonstrated that as the
341 adsorption time increases, the FTIR peak intensities of PS and PE exhibit an upward
342 trend, while those of PVC show no obvious change, indicating that the binding
343 interaction between PVC and NOMs is different from others [70]. This finding is
344 consistent with the obtained microscopic architectures of NPs–NOMs aggregates. In
345 addition, it has been deduced that if the surface sites of MPs are not rich enough, NOM
346 molecules will first occupy the adsorption sites on the surface of pristine MPs and then
347 bind to NOMs already retained on the MP, i.e., the multilayer adsorption mode, but if
348 there are sufficient binding sites on the surface of MPs, HA will tend to be bound as a
349 single layer [44, 71]. In our simulations, the binding of NOMs to NPs shows a structure
350 more resembling multilayer adsorption, possibly due to the similar size of both
351 substances.

352 To better visualize the microscopic aggregation structures, the solvent water
353 molecules are not shown in the snapshots. In fact, these water molecules are also
354 involved in the formation and stabilization of the supramolecular aggregates of NOMs–
355 NPs associations. Water molecules contribute to the intermolecular attraction between
356 NOMs and NPs fragments, where H–bonds and water bridges formed in both the outer
357 and inner domains of the clusters help to stabilize the hydrophilic functional groups, in

358 good agreement with earlier works [44, 72-74].

359

360 **Fig. 2.** Time evolution of solvent accessible surface areas (SASAs) of NOMs–NPs
361 associations in binary systems.

362

363 **Fig. 3.** Snapshots of NOMs–NPs heterogeneous aggregating clusters in binary systems.
364 Coloring code: N = blue; H = white; O = red; S = yellow; Ca = purple; Cl = orange.
365 Carbon atoms in NOMs and NPs are depicted in cyan and green, respectively.

366

367 3.2 Interaction energies between NOMs and NPs

368 The interaction energies between NOMs and pristine/aged NPs as a function of
369 simulation time are provided (Fig. S6) to clearly delineate the fundamental mechanism
370 leading to the spontaneous clustering and assembly of the two substances. For the
371 NOMs–pristine PE binary system (Fig. S6A), Coulombic energy is close to zero,
372 implying that electrostatic interaction is not favorable for the binding of NOMs to PE
373 particle, and in this case, only vdW interaction is responsible for the hetero–aggregation
374 behavior. For NOMs–virgin PVC and PS assemblages, both vdW and electrostatic
375 forces have contributions, with vdW interactions significantly stronger than
376 electrostatic interactions, suggesting that vdW interactions are the dominant driving
377 force responsible for aggregation between them and electrostatic interactions play a
378 very limited role; furthermore, electrostatic interaction is slightly more important in the
379 NOMs–PVC than in NOMs–PS system (Fig. S6C and E). In conclusion, vdW
380 interactions are mainly responsible for the binding and aggregation between NOMs and
381 unaged NPs, whereas the electrostatic driving force is only important for PVC. This
382 finding is in good agreement with recent studies [44, 75]. These differences can be
383 attributed to the chemical nature of the NP monomers, and our subsequent DFT
384 calculation results will give a direct interpretation of the observed difference.

385 Positive Coulombic interaction energies indicate unfavorable interactions between
386 NOMs and aged NPs (Fig. S6B, D, and F). This is because both substances are

387 negatively charged due to the deprotonation of carboxyl groups, resulting in an overall
388 repulsive force between them. For these systems, vdW interaction energies are slightly
389 negative (Fig. S6B, D, and F), implying that intermolecular forces mildly contribute to
390 the aggregation between NOMs and aged NPs. These results show that the direct
391 interaction between NOMs and aged NPs is not the dominant factor for their
392 aggregation behavior. Instead, the Ca^{2+} bridging effect attracting and binding to the
393 multiple deprotonated carboxylic groups plays a major role in promoting aggregation
394 (discussed below).

395 3.3. Local coordination by cation bridging

396 The bridging effect of cations such as Ca^{2+} has been recognized as a fundamental
397 mechanism for the stabilization and aggregation of NOM fragments that are abundant
398 in deprotonated carboxyl groups in near-neutral pH environments [5, 29, 76, 77]. In
399 comparison, the bridging effect between carboxyl groups of NOMs by Na^+ is relatively
400 weak, which means the aggregation of NOMs is not effectively promoted by Na^+ .
401 Consequently, Ca^{2+} cations in a water environment mainly contribute to the aggregation
402 behavior of NOMs and aged NPs. To quantitatively characterize the local coordination
403 structures of Ca^{2+} complexation with deprotonated carboxyl groups (COO^-) and to
404 distinguish Ca-bridged homogeneous and heterogeneous aggregation, radial
405 distribution functions (RDFs) were analyzed and presented.

406 Fig. S7 shows the RDFs curves of aqueous Ca^{2+} with respect to carboxyl O atoms
407 of NOMs and aged NPs, respectively, in binary systems. One can find that the scenarios
408 of Ca^{2+} coordination with carboxyl O of NOMs are very similar in all of the three
409 systems (Fig. S7A, C, and E). In brief, the RDF curves show a sharp and symmetrical
410 peak centered at $\sim 2.60 \text{ \AA}$, which corresponds to the average Ca–O^{carboxyl} bond length,
411 and the accumulating coordination number (CN) of the peak is around 2.1, which
412 indicates that, on average, each Ca^{2+} in solution binds firmly with 2.1 O atoms from
413 NOMs' carboxyl groups. Moreover, in the three binary systems, Ca^{2+} is respectively
414 bound to 0.92, 0.50, and 0.38 carboxyl O of aged PE, PS, and PVC with an average

415 distance of 2.60 Å (Fig. S7B, D, and F). These data show that when NOMs and aged
416 NPs coexist, homogeneous aggregation of both substances still occurs by Ca²⁺ bridging.

417 Fig. 4 shows the RDF and CN profiles of the C^{carboxyl} of NOMs surrounded by the
418 C^{carboxyl} of aged NPs, which helps to better reveal the heterogeneous aggregation
419 between them formed by Ca²⁺ bridging, and also illustrates representative
420 configurations corresponding to the peak positions of the RDF to visually show local
421 polymerizing structures of NOMs–NPs heterogeneous aggregation. A distinct peak or
422 multiple peaks between 3 and 6 Å can be identified in the carboxyl-carboxyl RDF
423 curves (Fig. 4A–C), and the accumulated CN values (at 6.0 Å) reveal that, on average,
424 each carboxyl group in NOMs is associated with 0.27, 0.16, and 0.10 carboxyl groups
425 in aged PE, PS, and PVC, forming multiple carboxyl chelates bridged by Ca²⁺ (Fig.
426 4D–F) and finally evolving into a heterogeneous aggregate.

427 To summarize, Ca²⁺ plays a crucial role in the aggregation (homogeneous and
428 heterogeneous) and stabilization of NOMs and aged NPs because the negatively
429 charged carboxyl groups are partially neutralized by Ca²⁺ cations in solution, which
430 reduces the intermolecular and intramolecular charge repulsion and limits
431 conformational expansion, thereby initializing the formation of compact aggregates.

432

433 **Fig. 4.** Radial distribution function (RDF) and coordination number (CN) curves of the
434 carboxyl C of NOMs with respect to the carboxyl C of aged NPs (A–C) and
435 representative hetero-polymerization structures bridged by Ca²⁺ (D–F). N = blue; H =
436 white; O = red; Ca = purple; Cl = orange. C atoms in NOMs and NPs are shown in cyan
437 and green, respectively.

438

439 3.4. Quantitative analysis of molecular surface by DFT calculations

440 3.4.1. Electrostatic potential

441 The isosurface-colored maps of electrostatic potential (ESP) (Fig. 5) are used to
442 characterize the overall ESP distributions of the six monomeric species of NPs. For
443 virgin PE, it can be found that due to its non-polar geometry, its vdW surface distributes

444 ESP of nearly zero evenly (Fig. 5A), resulting in the smallest magnitude of ESP among
445 all the NPs. Virgin PVC exhibits a significantly higher ESP scene, with the regions
446 around the Cl atom showing minimum negative ESP and the domains surrounding the
447 H atom presenting maximum positive values (Fig. 5B). Overall, virgin PS has a slightly
448 higher electronegativity than PE and the lowest ESPs, characterized by an annular
449 negative isosurface, are found in the regions between the benzene rings, while other
450 regions exhibit a significantly small magnitude of ESP (Fig. 5C).

451 Compared to the pristine NPs, the surface ESPs of the aged NPs are distributed in a
452 significantly lower region due to the introduction of non-uniformly distributed oxygen-
453 containing moieties, which are found to increase the non-uniform distribution of the
454 surface ESPs. This, together with the increased H–bonding interactions, promotes the
455 increase in adsorption and aggregation with NOMs. It can be clearly seen that the most
456 negative ESP values are caused by the deprotonated carboxylic groups in all three aged
457 NPs (Fig. 5D–F), indicating that these sites are prone to forming pronounced
458 electrostatic interactions with cations.

459

460 **Fig. 5.** Isosurface maps of the electrostatic potential (ESP) for (A) pristine PE, (B)
461 pristine PVC, (C) pristine PS, (D) aged PE, (E) aged PVC, and (F) aged PS (isosurface
462 = 0.001 a.u.). Red and blue colors correspond to the positive and negative parts of ESP,
463 respectively. Isosurface maps of vdW potential for (G) pristine PE, (H) pristine PVC,
464 and (I) pristine PS (isovalue = ± 0.75 kcal/mol). Green and blue colors correspond to
465 positive and negative values, respectively.

466

467 3.4.2. vdW potential

468 Due to the low polarity of pristine NPs, their vdW interaction should be of greater
469 importance in comparison to their electrostatic interaction according to chemical
470 intuition. Consequently, the isosurface maps of the vdW potentials of the three pristine
471 NPs are depicted. (Fig. 5G–I). This study primarily focused on the blue regions, where
472 the effect of dispersive attraction outweighs that of exchange–repulsion, and generally,
473 the interacting atoms bind to such region. For unaged PE, the negative part of its vdW

474 potential isosurface (blue region) is symmetrically distributed on both sides around C
475 atoms (Fig. 5G). Due to the negative ESP and the polarity generated by the Cl atoms in
476 virgin PVC, the blue region of its vdW potential isosurface is mainly concentrated
477 around C (Fig. 5H). For pristine PS, the blue region is predominantly near the ring
478 center (Fig. 5I). The strong dispersive attraction in this region suggests that π - π stacking
479 interaction plays a pivotal role in its aggregation with NOMs. In fact, strong π - π
480 interactions between PS and NOMs are clearly identified in the MD trajectories. An
481 earlier study also suggested the π - π conjugation for PS interaction with NOMs [23].

482 3.4.3. Molecular polarity index (MPI)

483 MPI is used to quantify the polarity of molecules with non-uniformly distributed
484 ESP. MPI is calculated by averaging the absolute values of ESPs on the surface of a
485 molecule. A higher MPI indicates a stronger polarity and a greater binding affinity
486 through electrostatic interactions. The calculated MPI values of the six NP monomers
487 are provided in Table S3, and for comparison, the MPI of water molecules is also
488 computed at the same theoretical level. The MPIs for unaged PE, PS, and PVC are 3.1,
489 8.5, and 22.2 kcal/mol, respectively. Therefore, PE exhibits the lowest polarity, and PS
490 also presents a very low polarity. As a result, it is mainly the vdW interactions, rather
491 than electrostatic interactions, that drive the aggregation of virgin PE and PS. In contrast,
492 the aged NPs are much more polar than their pristine forms, as the derived MPIs are
493 43.2 kcal/mol for aged PE, 51.6 kcal/mol for aged PS, and 42.2 kcal/mol for PVC. The
494 MPI of the H₂O molecule is found to be 22.1 kcal/mol, which is similar to that of
495 pristine PVC (22.2 kcal/mol) and much higher than that of pristine PE (3.1 kcal/mol)
496 and PS (8.5 kcal/mol). The MPI of H₂O is significantly lower than that of aged NPs (at
497 least 42.2 kcal/mol), and therefore the polarity of the water molecule is much smaller
498 than that of aged NPs, confirming that the strength of electrostatic interactions between
499 aged NPs and NOMs is rather weak.

500 3.5. Visualization analysis of weak interactions

501 Based on DFT calculations and wavefunction analysis, IGMH is a highly versatile
502 and effective analysis method for identifying and visualizing areas of significant
503 interaction in a wide range of chemical systems. An outstanding advantage of IGMH is
504 the ability to define fragments, so as to exclusively analyze the intermolecular
505 interactions between fragments. Taking the NOM-aged PS system as an example, the
506 DFT geometry optimization method was used to obtain the structure of NOM-aged PS
507 dimer with the initial configuration (1 aged PS molecule + 1 NOM fragment) from the
508 trajectory of MD simulations. According to the acquired structure, IGMH analysis of
509 the two fragments in such a dimer was carried out.

510 It can be seen that the isosurfaces between aged PS and NOM are largely green
511 (Fig. 6), which implies that slightly low electron density is in the region related to
512 intermolecular interaction, and the molecular binding between the two fragments is
513 predominantly induced by dispersion attraction, since electrostatic interaction normally
514 is accompanied by relatively higher electron density. Although the dispersion
515 interaction between atom pairs is typically assumed to be weak, the isosurfaces between
516 the fragments are notably wide, almost covering the whole interaction region (Fig. 6).
517 This observation could suggest that the vdW interaction between NOM and aged PS
518 fragments is not weak and play a significant role in the binding. Moreover, the
519 isosurfaces located between the rings of NOM and aged PS are stacked parallelly (Fig.
520 6), which signifies a significant π - π interaction. The π - π stacking effect is expected to
521 increase the binding strength. However, due to the big structural difference, there is no
522 comparable binding mode or interaction mechanism for PE and PVC. Hence, it can be
523 deduced that for other kinds of NPs that possess a benzene ring, π - π interaction is likely
524 to noticeably intensify their adhesion and aggregation with NOMs.

525

526 **Fig. 6.** $\text{Sign}(\lambda_2)\rho$ colored IGMH isosurface maps (of NOM-aged PS dimer. The NOM
527 monomer and PS monomer are defined as the two fragments in IGMH analysis. δg^{inter}
528 = 0.003 a.u.

529 4. Conclusion

530 This study investigated the dynamic aggregation and binding mechanisms
531 between NOMs and NPs at the molecular scale. Molecular modeling results showed
532 that the virgin NPs tend to form a homogeneous assembly, which is mainly driven by
533 hydrophobic force and vdW interaction. In contrast, due to the presence of negatively
534 charged carboxyl groups, the homogeneous aggregation of aged NPs is mainly caused
535 by the cation bridging effect, which partially neutralizes the negatively charged
536 carboxylic groups. Pristine PE and PS can easily assemble into a homogenous aggregate,
537 and then NOM molecules tend to be adsorbed on the outer surfaces of such NP particles,
538 then the subsequent NOMs can either bind to the NP surface sites or adhere to the NOM
539 fragments that have already been attached to the NPs. In comparison, NOM fragments
540 are not obviously adsorbed on the homogenous aggregate of virgin PVC due to its
541 relatively higher polarity and the presence of chlorine; instead, NOM molecules tend to
542 self-aggregate and then come into contact with the pristine PVC particle to form an
543 interface. In the case of aged NPs, their interactions with NOMs are governed by a
544 variety of mechanisms, such as intermolecular hydrogen bonding involving hydrophilic
545 functional groups, hydrophobic interactions including π - π stacking, and the cation
546 bridging effect.

547

548 CRediT authorship contribution statement

549 C.Z.: conceptualization, writing–original draft, writing–review & editing, investigation.
550 Z.Y.Z.: writing–original draft, writing–review & editing. M.N.X.: data curation,
551 software. H.Z.M.: data analysis. J.H.Q.: writing–review & editing, supervision,
552 resources. H.Z.J.: conceptualization, writing–review & editing, supervision, resources.

553 Declaration of Competing Interest

554 The authors declare that they have no known competing financial interests or personal
555 relationships that could have appeared to influence the work reported in this paper.

556 **Acknowledgements**

557 This work was supported by the National Natural Science Foundation of China (Grants
558 No. 42107263). We thank the High-Performance Computing Center (HPC) of
559 Northwest A&F University (NWAUFU) for providing computing resources and National
560 Center for Supercomputing in Xi'an.

561

562 **References**

- 563 [1] Kellerman, A. M.; Kothawala, D. N.; Dittmar, T.; Tranvik, L. J., Persistence of
564 dissolved organic matter in lakes related to its molecular characteristics. *Nat.*
565 *Geosci.* **2015**, *8*, (6), 454-457.
- 566 [2] Lehmann, J.; Kleber, M., The contentious nature of soil organic matter. *Nature*
567 **2015**, *528*, (7580), 60-68.
- 568 [3] Zhou, Z.; Zhang, C.; Xi, M.; Ma, H.; Jia, H., Multi-scale modeling of natural
569 organic matter–heavy metal cations interactions: Aggregation and stabilization
570 mechanisms. *Water Res.* **2023**, *238*, 120007.
- 571 [4] Lan, T.; Wu, P.; Yin, X.; Zhao, Y.; Liao, J.; Wang, D.; et al., Rigidity and Flexibility:
572 Unraveling the Role of Fulvic Acid in Uranyl Sorption on Graphene Oxide Using
573 Molecular Dynamics Simulations. *Environ. Sci. Technol.* **2023**, *57*, (28), 10339-
574 10347.
- 575 [5] Petrov, D.; Tunega, D.; Gerzabek, M. H.; Oostenbrink, C., Molecular Dynamics
576 Simulations of the Standard Leonardite Humic Acid: Microscopic Analysis of the
577 Structure and Dynamics. *Environ. Sci. Technol.* **2017**, *51*, (10), 5414-5424.
- 578 [6] Ali, I.; Tan, X.; Li, J.; Peng, C.; Naz, I.; Duan, Z.; et al., Interaction of microplastics
579 and nanoplastics with natural organic matter (NOM) and the impact of NOM on
580 the sorption behavior of anthropogenic contaminants – A critical review. *Journal*
581 *of Cleaner Production* **2022**, *376*, 134314.
- 582 [7] Jambeck, J. R.; Geyer, R.; Wilcox, C.; Siegler, T. R.; Perryman, M.; Andrady, A.;
583 et al., Plastic waste inputs from land into the ocean. *Science* **2015**, *347*, (6223),
584 768-771.
- 585 [8] Gewert, B.; Plassmann, M. M.; MacLeod, M., Pathways for degradation of plastic
586 polymers floating in the marine environment. *Environ Sci Process Impacts* **2015**,
587 *17*, (9), 1513-21.
- 588 [9] Moharir, R. V.; Kumar, S., Challenges associated with plastic waste disposal and
589 allied microbial routes for its effective degradation: A comprehensive review.
590 *Journal of Cleaner Production* **2019**, *208*, 65-76.
- 591 [10] Hu, D.; Shen, M.; Zhang, Y.; Zeng, G., Micro(nano)plastics: An un-ignorable
592 carbon source? *Sci. Total Environ.* **2019**, *657*, 108-110.
- 593 [11] Liu, G.; Zhu, Z.; Yang, Y.; Sun, Y.; Yu, F.; Ma, J., Sorption behavior and
594 mechanism of hydrophilic organic chemicals to virgin and aged microplastics in

- 595 freshwater and seawater. *Environ. Pollut.* **2019**, *246*, 26-33.
- 596 [12] Wang, Q.; Zhang, Y.; Wangjin, X.; Wang, Y.; Meng, G.; Chen, Y., The adsorption
597 behavior of metals in aqueous solution by microplastics effected by UV radiation.
598 *J. Environ. Sci. (China)* **2020**, *87*, 272-280.
- 599 [13] Shen, M.; Zhu, Y.; Zhang, Y.; Zeng, G.; Wen, X.; Yi, H.; et al., Micro(nano)plastics:
600 Unignorable vectors for organisms. *Mar. Pollut. Bull.* **2019**, *139*, 328-331.
- 601 [14] Pradel, A.; Catrouillet, C.; Gigault, J., The environmental fate of nanoplastics:
602 What we know and what we need to know about aggregation. *NanoImpact* **2023**,
603 *29*, 100453.
- 604 [15] Alimi, O. S.; Farner Budarz, J.; Hernandez, L. M.; Tufenkji, N., Microplastics and
605 Nanoplastics in Aquatic Environments: Aggregation, Deposition, and Enhanced
606 Contaminant Transport. *Environ. Sci. Technol.* **2018**, *52*, (4), 1704-1724.
- 607 [16] Gigault, J.; El Hadri, H.; Nguyen, B.; Grassl, B.; Roweczyk, L.; Tufenkji, N.; et
608 al., Nanoplastics are neither microplastics nor engineered nanoparticles. *Nature*
609 *Nanotechnology* **2021**, *16*, (5), 501-507.
- 610 [17] Lambert, S.; Wagner, M., Characterisation of nanoplastics during the degradation
611 of polystyrene. *Chemosphere* **2016**, *145*, 265-268.
- 612 [18] Liu, Y.; Wang, Y.; Ling, X.; Yan, Z.; Wu, D.; Liu, J.; et al., Effects of Nanoplastics
613 and Butyl Methoxydibenzoylmethane on Early Zebrafish Embryos Identified by
614 Single-Cell RNA Sequencing. *Environ. Sci. Technol.* **2021**, *55*, (3), 1885-1896.
- 615 [19] Wang, Z.; Xing, X.; Xue, M.; Bai, S.; Li, P.; Li, C.; et al., Insights into
616 heteroaggregation of polystyrene nanoplastics with hematite nanoparticles and
617 configuration-dependent adsorption for PFOA and PFOS. *Colloids Surf., A* **2022**,
618 *649*, 129467.
- 619 [20] Zhang, Y.; Luo, Y.; Yu, X.; Huang, D.; Guo, X.; Zhu, L., Aging significantly
620 increases the interaction between polystyrene nanoplastic and minerals. *Water Res.*
621 **2022**, *219*, 118544.
- 622 [21] Mao, Y.; Li, H.; Huangfu, X.; Liu, Y.; He, Q., Nanoplastics display strong stability
623 in aqueous environments: Insights from aggregation behaviour and theoretical
624 calculations. *Environ. Pollut.* **2020**, *258*, 113760.
- 625 [22] Singh, N.; Tiwari, E.; Khandelwal, N.; Darbha, G. K., Understanding the stability
626 of nanoplastics in aqueous environments: effect of ionic strength, temperature,
627 dissolved organic matter, clay, and heavy metals. *Environmental Science: Nano*
628 **2019**, *6*, (10), 2968-2976.
- 629 [23] Ding, L.; Luo, Y.; Yu, X.; Ouyang, Z.; Liu, P.; Guo, X., Insight into interactions of
630 polystyrene microplastics with different types and compositions of dissolved
631 organic matter. *Sci. Total Environ.* **2022**, *824*, 153883.
- 632 [24] Yin, Y.; Shen, M.; Tan, Z.; Yu, S.; Liu, J.; Jiang, G., Particle coating-dependent
633 interaction of molecular weight fractionated natural organic matter: impacts on the
634 aggregation of silver nanoparticles. *Environ. Sci. Technol.* **2015**, *49*, (11), 6581-9.
- 635 [25] Oriekhova, O.; Stoll, S., Heteroaggregation of nanoplastic particles in the presence
636 of inorganic colloids and natural organic matter. *Environmental Science: Nano*

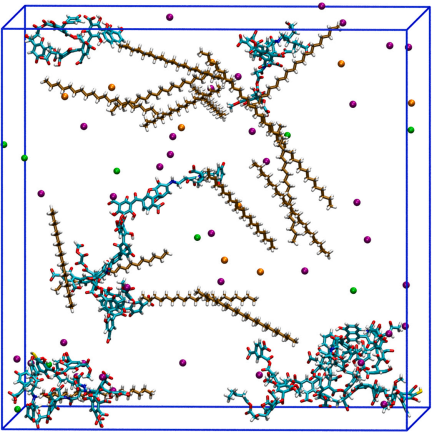
- 637 **2018**, 5, (3), 792-799.
- 638 [26] Greathouse, J.; Johnson, K.; Greenwell, H., Interaction of Natural Organic Matter
639 with Layered Minerals: Recent Developments in Computational Methods at the
640 Nanoscale. *Minerals* **2014**, 4, (2), 519-540.
- 641 [27] Devarajan, D.; Liang, L.; Gu, B.; Brooks, S. C.; Parks, J. M.; Smith, J. C.,
642 Molecular Dynamics Simulation of the Structures, Dynamics, and Aggregation of
643 Dissolved Organic Matter. *Environ. Sci. Technol.* **2020**, 54, (21), 13527-13537.
- 644 [28] Kalinichev, A. G.; Iskrenova-Tchoukova, E.; Ahn, W. Y.; Clark, M. M.;
645 Kirkpatrick, R. J., Effects of Ca²⁺ on supramolecular aggregation of natural
646 organic matter in aqueous solutions: A comparison of molecular modeling
647 approaches. *Geoderma* **2011**, 169, 27-32.
- 648 [29] Zhang, Y.; Liu, X.; Zhang, C.; Lu, X., A combined first principles and classical
649 molecular dynamics study of clay-soil organic matters (SOMs) interactions.
650 *Geochim. Cosmochim. Acta* **2020**, 291, 110-125.
- 651 [30] Liang, J.; Zhen, P.; Gan, P.; Li, Y.; Tong, M.; Liu, W., DFT Calculation of
652 Nonperiodic Small Molecular Systems to Predict the Reaction Mechanism of
653 Advanced Oxidation Processes: Challenges and Perspectives. *ACS ES&T*
654 *Engineering* **2023**.
- 655 [31] Li, F.; Borthwick, A. G. L.; Liu, W., Environmental theoretical calculation for non-
656 periodic systems. *Trends in Chemistry* **2023**, 5, (6), 410-414.
- 657 [32] He, M.; Liu, X.; Lu, X.; Zhang, Y.; Wang, R., Structure, Stability, and Acidity of
658 the Uranyl Arsenate Dimer in Aqueous Solution. *Inorg. Chem.* **2023**, 62, (22),
659 8729-8738.
- 660 [33] He, M.; Liu, X.; Cheng, J.; Lu, X.; Zhang, C.; Wang, R., Uranyl Arsenate
661 Complexes in Aqueous Solution: Insights from First-Principles Molecular
662 Dynamics Simulations. *Inorg. Chem.* **2018**, 57, (10), 5801-5809.
- 663 [34] Xue, Q.; Jiao, Z.; Pan, W.; Liu, X.; Fu, J.; Zhang, A., Multiscale computational
664 simulation of pollutant behavior at water interfaces. *Water Res.* **2024**, 250, 121043.
- 665 [35] Chen, Y.; Li, H.; Yin, Y.; Shan, S.; Huang, T.; Tang, H., Effect of microplastics on
666 the adherence of coexisting background organic contaminants to natural organic
667 matter in water. *Sci. Total Environ.* **2023**, 905, 167175.
- 668 [36] Zhu, K.; Jia, H.; Zhao, S.; Xia, T.; Guo, X.; Wang, T.; et al., Formation of
669 Environmentally Persistent Free Radicals on Microplastics under Light Irradiation.
670 *Environ. Sci. Technol.* **2019**, 53, (14), 8177-8186.
- 671 [37] Luo, Y.; Zhang, Y.; Xu, Y.; Guo, X.; Zhu, L., Distribution characteristics and
672 mechanism of microplastics mediated by soil physicochemical properties. *Sci.*
673 *Total Environ.* **2020**, 726, 138389.
- 674 [38] Zhu, K.; Sun, Y.; Jiang, W.; Zhang, C.; Dai, Y.; Liu, Z.; et al., Inorganic anions
675 influenced the photoaging kinetics and mechanism of polystyrene microplastic
676 under the simulated sunlight: Role of reactive radical species. *Water Res.* **2022**,
677 216, 118294.
- 678 [39] Escalona, Y.; Petrov, D.; Oostenbrink, C., Vienna soil organic matter modeler 2

- 679 (VSOMM2). *J. Mol. Graphics Modell.* **2021**, *103*, 107817.
- 680 [40] Sündermann, A.; Solc, R.; Tunega, D.; Haberhauer, G.; Gerzabek, M. H.;
681 Oostenbrink, C., Vienna Soil-Organic-Matter Modeler—Generating condensed-
682 phase models of humic substances. *J. Mol. Graphics Modell.* **2015**, *62*, 253-261.
- 683 [41] Chen, Y.; Tang, H.; Cheng, Y.; Huang, T.; Xing, B., Interaction between
684 microplastics and humic acid and its effect on their properties as revealed by
685 molecular dynamics simulations. *J. Hazard. Mater.* **2023**, *455*, 131636.
- 686 [42] Van Der Spoel, D.; Lindahl, E.; Hess, B.; Groenhof, G.; Mark, A. E.; Berendsen,
687 H. J., GROMACS: fast, flexible, and free. *J. Comput. Chem.* **2005**, *26*, (16), 1701-
688 18.
- 689 [43] Duan, Y.; Wu, C.; Chowdhury, S.; Lee, M. C.; Xiong, G.; Zhang, W.; et al., A point-
690 charge force field for molecular mechanics simulations of proteins based on
691 condensed-phase quantum mechanical calculations. *J. Comput. Chem.* **2003**, *24*,
692 (16), 1999-2012.
- 693 [44] Essmann, U.; Perera, L.; Berkowitz, M. L.; Darden, T.; Lee, H.; Pedersen, L. G.,
694 A smooth particle mesh Ewald method. *J. Chem. Phys.* **1995**, *103*, (19), 8577-8593.
- 695 [45] Berendsen, H. J. C.; Grigera, J. R.; Straatsma, T. P., The missing term in effective
696 pair potentials. *J. Phys. Chem. C* **1987**, *91*, (24), 6269-6271.
- 697 [46] Hess, B.; Bekker, H.; Berendsen, H. J. C.; Fraaije, J. G. E. M., LINCS: A linear
698 constraint solver for molecular simulations. **1997**, *18*, (12), 1463-1472.
- 699 [47] Berendsen; Postma, J. P. M.; van Gunsteren, W. F.; DiNola, A.; Haak, J. R.,
700 Molecular dynamics with coupling to an external bath. *J. Chem. Phys.* **1984**, *81*,
701 (8), 3684-3690.
- 702 [48] Bussi, G.; Donadio, D.; Parrinello, M., Canonical sampling through velocity
703 rescaling. *J. Chem. Phys.* **2007**, *126*, (1), 014101.
- 704 [49] Weigend, F.; Ahlrichs, R., Balanced basis sets of split valence, triple zeta valence
705 and quadruple zeta valence quality for H to Rn: Design and assessment of accuracy.
706 *Phys. Chem. Chem. Phys.* **2005**, *7*, (18), 3297-305.
- 707 [50] Becke, A. D., Density-functional thermochemistry. III. The role of exact exchange.
708 *J. Chem. Phys.* **1993**, *98*, (7), 5648-5652.
- 709 [51] Lee, C.; Yang, W.; Parr, R. G., Development of the Colle-Salvetti correlation-
710 energy formula into a functional of the electron density. *Phys Rev B Condens*
711 *Matter* **1988**, *37*, (2), 785-789.
- 712 [52] Grimme, S.; Antony, J.; Ehrlich, S.; Krieg, H., A consistent and accurate ab initio
713 parametrization of density functional dispersion correction (DFT-D) for the 94
714 elements H-Pu. *J. Chem. Phys.* **2010**, *132*, (15), 154104.
- 715 [53] Lu, T.; Chen, F., Multiwfn: a multifunctional wavefunction analyzer. *J. Comput.*
716 *Chem.* **2012**, *33*, (5), 580-92.
- 717 [54] Schauerl, M.; Nerenberg, P. S.; Jang, H.; Wang, L.-P.; Bayly, C. I.; Mobley, D.
718 L.; et al., Non-bonded force field model with advanced restrained electrostatic
719 potential charges (RESP2). *Communications Chemistry* **2020**, *3*, (1), 44.
- 720 [55] Bader, R. F. W.; Carroll, M. T.; Cheeseman, J. R.; Chang, C., Properties of atoms

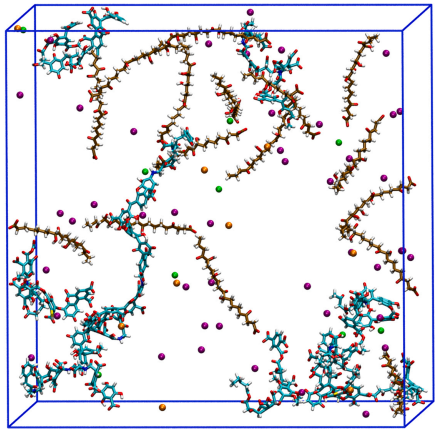
- 721 in molecules: atomic volumes. *J. Am. Chem. Soc.* **1987**, *109*, (26), 7968-7979.
- 722 [56] Lu, T.; Chen, Q., van der Waals potential: an important complement to molecular
723 electrostatic potential in studying intermolecular interactions. *J. Mol. Model.* **2020**,
724 *26*, (11), 315.
- 725 [57] Lu, T.; Chen, Q., Independent gradient model based on Hirshfeld partition: A new
726 method for visual study of interactions in chemical systems. **2022**, *43*, (8), 539-
727 555.
- 728 [58] Humphrey, W.; Dalke, A.; Schulten, K., VMD: Visual molecular dynamics. *J. Mol.*
729 *Graphics* **1996**, *14*, (1), 33-38.
- 730 [59] Kuehne, T. D.; Iannuzzi, M.; Del Ben, M.; Rybkin, V. V.; Seewald, P.; Stein, F.; et
731 al., CP2K: An electronic structure and molecular dynamics software package -
732 Quickstep: Efficient and accurate electronic structure calculations. *J. Chem. Phys.*
733 **2020**, *152*, (19).
- 734 [60] Lippert, B. G.; Hutter, J.; Parrinello, M., A hybrid Gaussian and plane wave density
735 functional scheme. *Mol. Phys.* **1997**, *92*, (92), 477-487.
- 736 [61] Perdew, J. P.; Burke, K.; Ernzerhof, M., Generalized gradient approximation made
737 simple. *Phys. Rev. Lett.* **1996**, *77*, (18), 3865-3868.
- 738 [62] VandeVondele, J.; Hutter, J., Gaussian basis sets for accurate calculations on
739 molecular systems in gas and condensed phases. *J. Chem. Phys.* **2007**, *127*, (11),
740 114105.
- 741 [63] Goedecker, S.; Teter, M.; Hutter, J., Separable dual-space Gaussian
742 pseudopotentials. *Phys. Rev. B: Condens. Matter* **1996**, *54*, (3), 1703--1710.
- 743 [64] Byrd, R. H.; Lu, P.; Nocedal, J.; Zhu, C., A Limited Memory Algorithm for Bound
744 Constrained Optimization. **1995**, *16*, (5), 1190-1208.
- 745 [65] Andreussi, O.; Dabo, I.; Marzari, N., Revised self-consistent continuum solvation
746 in electronic-structure calculations. *J. Chem. Phys.* **2012**, *136*, (6).
- 747 [66] Sun, Q., The Hydrophobic Effects: Our Current Understanding. *Molecules* **2022**,
748 *27*, (20).
- 749 [67] Aquino, A. J. A.; Tunega, D.; Schaumann, G. E.; Haberhauer, G.; Gerzabek, M.
750 H.; Lischka, H., The functionality of cation bridges for binding polar groups in
751 soil aggregates. *Int. J. Quantum Chem* **2010**, *111*, (7-8), 1531-1542.
- 752 [68] Galicia-Andrés, E.; Oostenbrink, C.; Gerzabek, M. H.; Tunega, D., On the
753 Adsorption Mechanism of Humic Substances on Kaolinite and Their Microscopic
754 Structure. *Minerals* **2021**, *11*, (10).
- 755 [69] Escalona, Y.; Petrov, D.; Galicia-Andrés, E.; Oostenbrink, C., Exploring the
756 Macroscopic Properties of Humic Substances Using Modeling and Molecular
757 Simulations. *Agronomy* **2023**, *13*, (4).
- 758 [70] Wang, X.; Wang, X.; Zhu, W.; Ding, L.; Liang, X.; Wu, R.; et al., Insight into
759 interactions between microplastics and fulvic acid: Mechanisms affected by
760 microplastics type. *Sci. Total Environ.* **2024**, *913*, 169427.
- 761 [71] Abdurahman, A.; Cui, K.; Wu, J.; Li, S.; Gao, R.; Dai, J.; et al., Adsorption of
762 dissolved organic matter (DOM) on polystyrene microplastics in aquatic

- 763 environments: Kinetic, isotherm and site energy distribution analysis. *Ecotoxicol.*
764 *Environ. Saf.* **2020**, *198*, 110658.
- 765 [72] Aquino, A. J. A.; Tunega, D.; Pašalić, H.; Schaumann, G. E.; Haberhauer, G.;
766 Gerzabek, M. H.; et al., Molecular Dynamics Simulations of Water Molecule-
767 Bridges in Polar Domains of Humic Acids. *Environ. Sci. Technol.* **2011**, *45*, (19),
768 8411-8419.
- 769 [73] Kučerík, J.; Ondruch, P.; Kunhi Mouvenchery, Y.; Schaumann, G. E., Formation
770 of Water Molecule Bridges Governs Water Sorption Mechanisms in Soil Organic
771 Matter. *Langmuir* **2018**, *34*, (40), 12174-12182.
- 772 [74] Boyle, M.; Frankenberger Jr., W. T.; Stolzy, L. H., The Influence of Organic Matter
773 on Soil Aggregation and Water Infiltration. **1989**, *2*, (4), 290-299.
- 774 [75] Liu, W.; Tang, H.; Yang, B.; Li, C.; Chen, Y.; Huang, T., Molecular level insight
775 into the different interaction intensity between microplastics and aromatic
776 hydrocarbon in pure water and seawater. *Sci. Total Environ.* **2023**, *862*, 160786.
- 777 [76] Iskrenova-Tchoukova, E.; Kalinichev, A. G.; Kirkpatrick, R. J., Metal Cation
778 Complexation with Natural Organic Matter in Aqueous Solutions: Molecular
779 Dynamics Simulations and Potentials of Mean Force. *Langmuir* **2010**, *26*, (20),
780 15909-15919.
- 781 [77] Kalinichev, A. G.; Kirkpatrick, R. J., Molecular dynamics simulation of cationic
782 complexation with natural organic matter. **2007**, *58*, (4), 909-917.

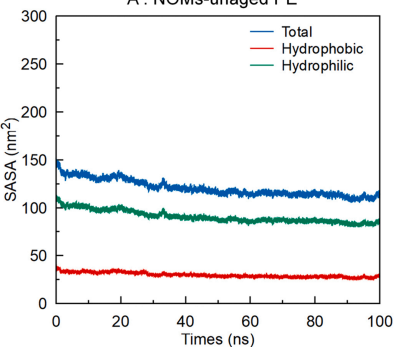
A: NOMs-unaged NPs



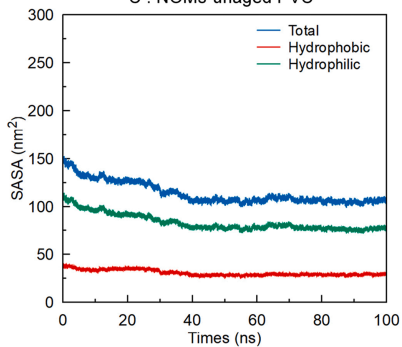
B: NOMs-aged NPs



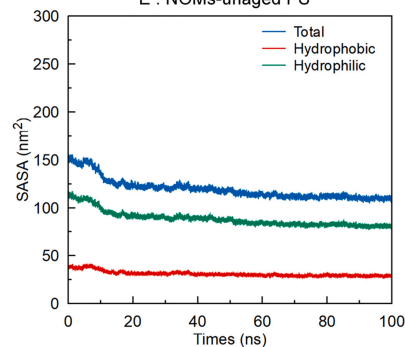
A : NOMs-unaged PE



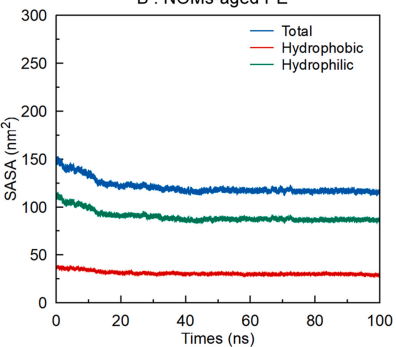
C : NOMs-unaged PVC



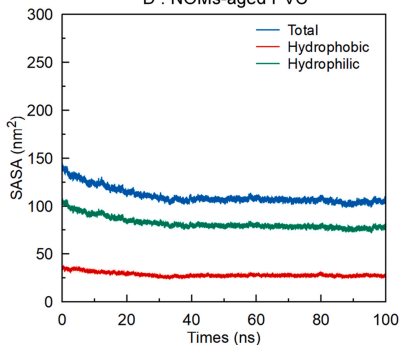
E : NOMs-unaged PS



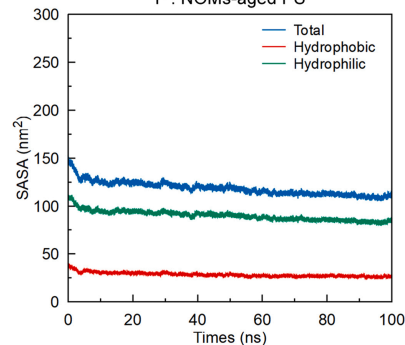
B : NOMs-aged PE



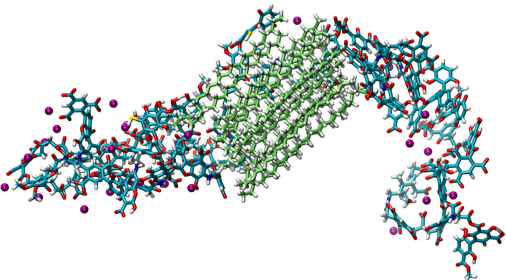
D : NOMs-aged PVC



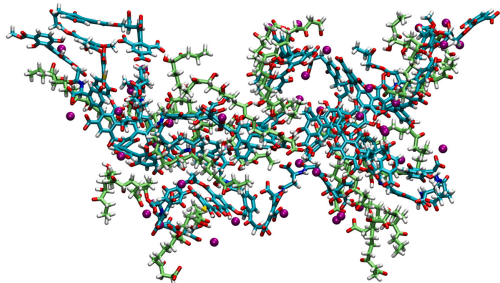
F : NOMs-aged PS



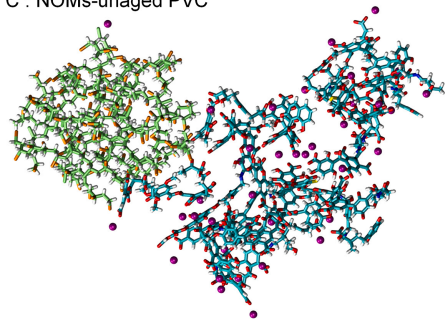
A : NOMs-unaged PE



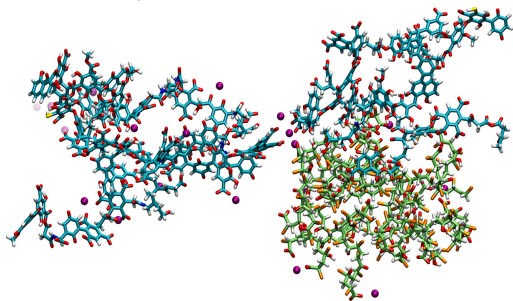
B : NOMs-aged PE



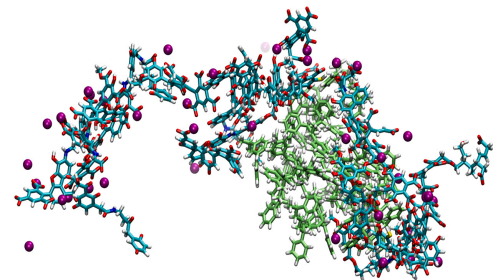
C : NOMs-unaged PVC



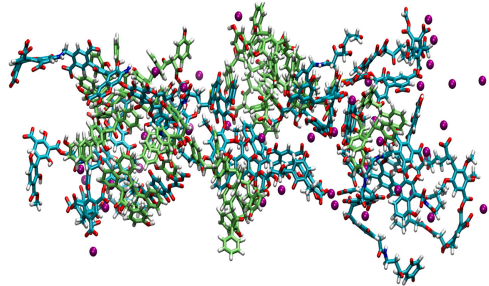
D : NOMs-aged PVC



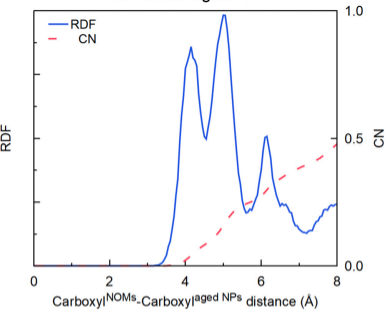
E : NOMs-unaged PS



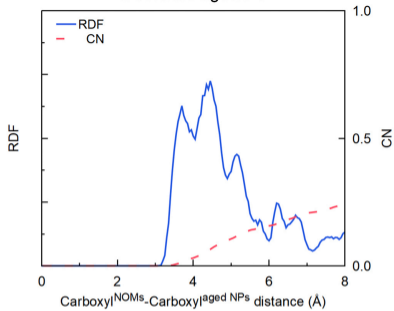
F : NOMs-aged PS



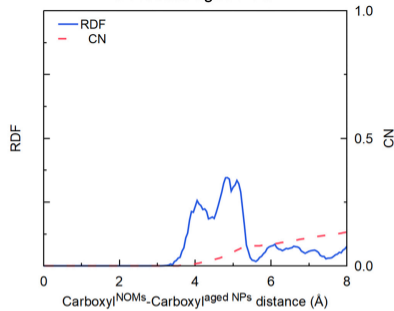
A : NOMs-aged PE



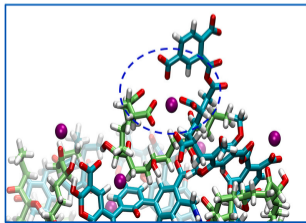
B : NOMs-aged PS



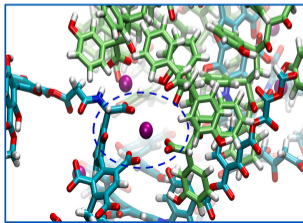
C : NOMs-aged PVC



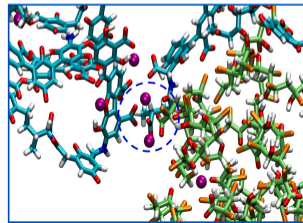
D : NOMs-aged PE association



E : NOMs-aged PS association

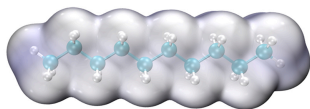


F : NOMs-aged PVC association

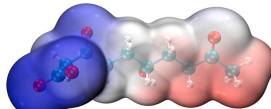


Electrostatic potential

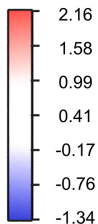
A: pristine PE



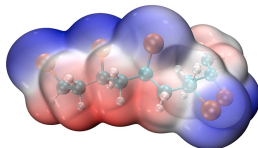
D: aged PE



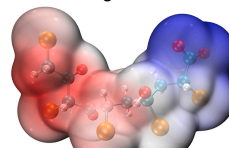
ESP (eV)



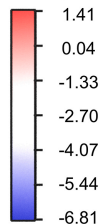
B: pristine PVC



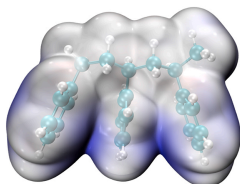
E: aged PVC



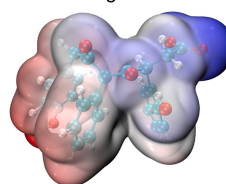
ESP (eV)



C: pristine PS

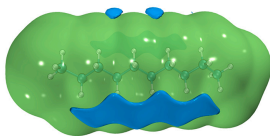


F: aged PS

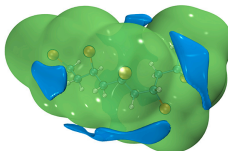


vdW potentials

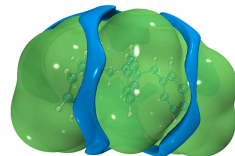
G: pristine PE

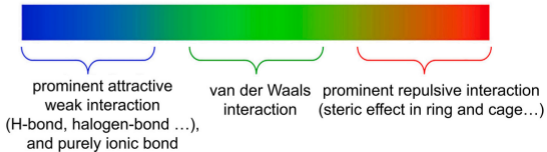
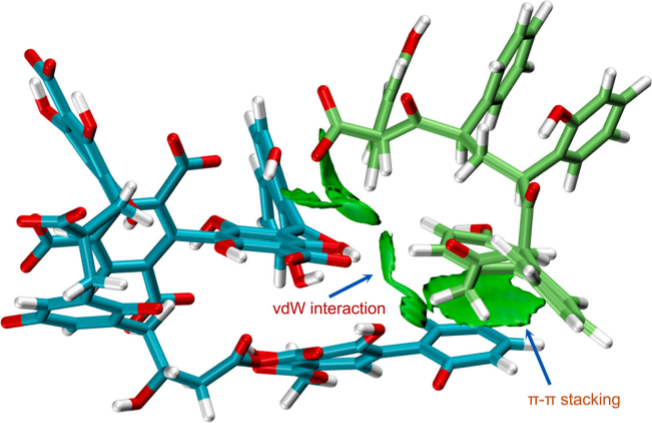


H: pristine PVC



I: pristine PS





Highlights:

- NOMs–NPs interactions were revealed by multi-scale computational modeling
- Advanced NOMs models created by VSOMM2 were used in simulations.
- Dynamic aggregation mechanisms were elucidated and quantified.
- Pristine and aged NPs show dissimilar aggregation mechanisms.
- PE, PS, and PVC aggregation with NOMs occur via different processes.